Heliyon 10 (2024) e39966

Contents lists available at ScienceDirect

Heliyon

journal homepage: www.cell.com/heliyon

Research article

Carbon nanotube-Yttrium iron garnet nanohybrid synthesized via chemical vapor deposition and its potential application in fabricated screen-printed patch antenna

Intan Helina Hasan [a,*], Ismayadi Ismail [a], Mohd Nizar Hamidon [a,b], Muhammad Syazwan Mustaffa [a], Nor Hapishah Abdullah [a], Farah Nabilah Shafiee [a]

[a] Institute of Nanoscience and Nanotechnology, Universiti Putra Malaysia, 43400, UPM Serdang, Selangor, Malaysia
[b] Faculty of Engineering, Universiti Putra Malaysia, 43400, UPM Serdang, Selangor, Malaysia

ARTICLE INFO

Keywords:
Nanohybrid
Thick film
Patch antenna
Carbon
Ferrites

ABSTRACT

Carbon nanotube-Yttrium iron garnet (CNT-YIG) nanohybrid has been successfully synthesized using chemical vapor deposition (CVD) with yttrium iron garnet (YIG) nanopowders as catalyst, ethanol as carbon stock, and argon as carrier gas. Carbon nanotube (CNT) was observed to have grown from the YIG nanopowders with bamboo-like structures of CNT at a synthesis temperature of 900 °C. FESEM and RAMAN characterization indicated that the CNT-YIG nanohybrid exhibited the growth of bamboo-like CNT with high graphitization. Further analysis of electrical properties showed that the CNT-YIG nanohybrid has exhibited conductivity due to the CNT growth. The nanohybrid in the form of powders was then mixed with an organic vehicle to produce thick film paste and screen-printed onto a substrate as the working material for patch antenna application. Initial measurements using VNA indicated that CNT-YIG nanohybrid gave significant results regarding return loss and bandwidth, proving that the materials could have great potential to enhance patch antenna performance due to their combined electrical and magnetic properties.

1. Introduction

Carbon-based materials are gaining popularity in research communities around the globe, particularly because of their exciting and somewhat mysterious properties covering mechanical, chemical, electrical, and many others. Thousands of papers have been discussing and studying the properties of these materials, specifically those in the nanoscale region, for example, carbon nanotube (CNT), graphene, and carbon quantum dot (CQD). Particularly for CNT, its excellent electrical properties, such as high conductivity, prompted much research work on CNT-based antennas. Hanson explored the properties of CNT-based dipole antennas since the CNT can be grown up to several centimeters in length [1,2]. Such small-scale antennas, or what is termed a nanoantenna, can be used for microscopic or nanoscopic circuits and systems.

Later, a few researchers started to explore the use of CNT as the conductive material in the fabrication of microstrip patch antennas [3–11]. Elwi et al. have demonstrated the fabrication of a multi-walled CNT (MWCNT) microstrip patch antenna by producing MWCNT ink and using the inkjet printing method to print the conductive patch onto a substrate [3]. The results have exhibited that CNT-based patch antennas can obtain good results on top of having a wider bandwidth due to their ability to conduct microwave energy via the

* Corresponding author.
E-mail address: i_helina@upm.edu.my (I.H. Hasan).

https://doi.org/10.1016/j.heliyon.2024.e39966
Received 12 August 2024; Received in revised form 23 October 2024; Accepted 29 October 2024
Available online 30 October 2024

structures of CNT itself. The most recent interesting work was the development of microcellular-structured CNT films with enhanced microwave absorption capability, having an effective bandwidth of 11.5 GHz [12]. This proved that the work can be further explored, specifically for harsh environments, due to its non-corrosive and non-oxidizing properties.

Meanwhile, ferrites have been proven to help in further improving the performance of the patch antenna, either as a substrate or as a form of overlay film as part of the patch antenna [13–21]. Our previous work has demonstrated that the ferrite material can be introduced as a thick film layer in between the conductive patch and the substrate using a screen-printing technique to widen the frequency bandwidth, as well as improving the return loss of the patch antenna [22,23]. Based on this literature, there were possibilities that when both conductive and magnetic materials were combined or mixed to form the patch of the antenna, better performance could be observed and manipulated. Some researchers have successfully demonstrated that the idea can work in relation to microwave applications [24–30]. Most of the work has produced the CNT-ferrite nanocomposite by mixing the two materials or using other methods to combine them together, such as the chemical vapor deposition method (CVD) [31,32], melt bending process [33], in the form of a three-dimensional hybrid aerogel [34], one-pot coprecipitation [35–37], and homogeneous precipitation [38].

Realizing the great potential of CNT-ferrite nanocomposite, we demonstrated the synthesis of CNT-YIG nanohybrid via the CVD method by growing CNT onto YIG nanopowders. The novelty and advantage of this work is that, in theory, this nanohybrid material would exhibit electrical, dielectric, and magnetic properties and can be further explored as a material for a fabricated screen-printed microstrip patch antenna in hopes of improving the performance in terms of return loss and bandwidth. Particularly, the novelty of utilizing CNT-YIG nanohybrid as the radiating patch antenna is that the enhanced properties of the nanomaterials by combining the electrical conductivity of CNT and the low-loss magnetic properties of the YIG can increase the electrical and magnetic field of the radiating patch, therefore improving the return loss and the bandwidth of the antenna.

2. Materials and methods

CNT-YIG nanohybrid was prepared using YIG nanopowders purchased from Sigma-Aldrich (nanopowder, <100 nm particle size (BET), 99.9 % trace metal basis) as the catalyst for CNT growth via CVD. They were initially characterized by using a Raman spectroscopy (Witec, Alpha 300R) and a field emission scanning electron microscope (FESEM) (FEI, Nova NanoSEM 450) as starting powders. The nanopowders were put into an alumina boat at the center of the furnace with a starting weight of 0.5 g. The furnace was then flushed with argon gas at 100 sccm. The furnace was then heated to the targeted temperature, which was 900 °C. The synthesis temperature was chosen based on the maximum temperature of the CVD used and the range within which the carbon atoms can move slowly and form non-hexagonal carbon rings [39]. After the furnace had reached the targeted temperature, ethanol was injected into the furnace as the hydrocarbon source with a constant flow of 10 ml/h by using a syringe pump under argon gas flow. After the process was completed, the furnace was then cooled down to room temperature before the samples were collected for further analysis. Samples were characterized using a Raman spectroscopy, an X-ray diffractometer (XRD) (Rigaku, SmartLab 2 MiniFlex 600), and FESEM to study the graphitization of the samples, phase formation, and morphological structures of the nanohybrid, while the structural analysis of the CNT grown from the nanopowders was observed using a high-resolution transmission electron microscope (HRTEM) (JEOL JEM 2100F). The electromagnetic properties of the samples were then measured using a vector network analyzer (VNA) (Agilent, N5227A).

Later, the samples were used as the active element for thick film paste preparation. The CNT-YIG nanohybrid powders were mixed with an organic binder with a powder-to-binder ratio of 30:70 wt%. The organic binder consisted of linseed stand oil, m-xylene, and alpha-terpineol, with a composition as explained in Ref. [23], which was prepared beforehand. The powders and organic binder were mixed using a magnetic stirrer at a speed of 250 rpm for 5 h continuously at a temperature of 40 °C to obtain a homogenous paste. The paste was then left overnight to allow it to settle down, and then printed onto an alumina substrate, dried, and fired at 300 °C to produce a 20 μm-thick film [40]. The I-V characteristics of the thick film samples were measured using a 2-point probe (Keithley 2450), while the conductivity, resistivity, and sheet resistance were measured using a Mitsubishi Loresta GX (MCP-T700) resistivity meter,

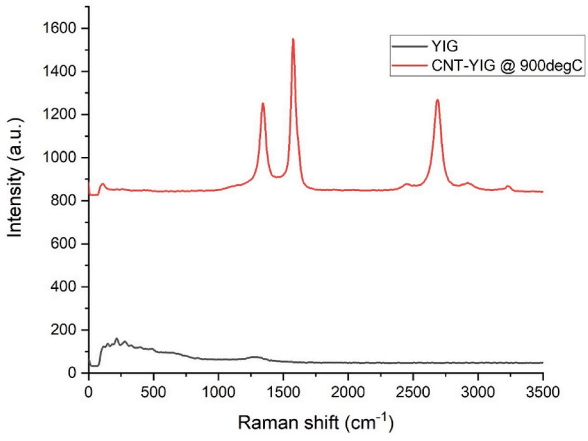

Fig. 1. Raman shifts of YIG nanopowders and CNT-YIG nanohybrid powders synthesized at 900 °C using CVD.

which uses the 4-terminal, 4-pin method (4-point probe).

To investigate the resonance frequency and return loss of the material in the form of patch antenna , the antenna was fabricated using the CNT-YIG nanohybrid thick film paste as the conductive patch and FR4 as the substrate. The antenna utilized the design discovered in previous work [23,41] for comparison purposes. Once the fabrication was completed, the antenna was tested using VNA to measure the frequency and return loss (S_{11} parameter) in the range of 2–14 GHz.

3. Results and discussion

3.1. Raman spectroscopy analysis

When the CVD process was carried out at a temperature of 900 °C, three distinctive peaks were observed using Raman spectroscopy (see Fig. 1). The first peak was the D band, which originated from the defects in the sidewalls and ends of CNT and was identified at 1341 cm^{-1}. The second peak, which was the G band, was derived from the tangential stretching of the carbon-carbon band located at 1574 cm^{-1}. Meanwhile, a G' band located at 2700 cm^{-1} was an overtone of the D peak [42]. The sharp and distinctive peaks of the D band and G band, with the G band peak being higher than the D band, indicated that the CNT was graphitic, which showed good growth of the CNT. The ratio of D/G peak intensities (I_D/I_G) was conventionally used to estimate the degree of defectiveness of graphene layers in CNT. The I_D/I_G ratio of CNT-YIG synthesized was 0.75, indicating that the CNT-YIG produced had fewer defects, which therefore hypothetically favored the electron mobility in the materials. The G' band, sometimes referred to as the 2D band, was also visible, with a distinctive peak showing that the CNT had fewer walls. The radial breathing mode (RBM) was not detected, hence indicating that the samples were multiwalled CNT.

3.2. Phase and microstructural analysis

XRD analysis was performed to investigate the phase formation of the synthesized CNT-YIG nanohybrid (Fig. 2). The XRD spectrum of YIG nanopowders revealed that there were two types of YIG phases that existed in the powders: orthorhombic YIG with the chemical formula $Y_3Fe_5O_{12}$ (DB card no. 00-021-1450), and cubic YIG with the chemical formula $Y_3Fe_2(FeO_4)_3$ (DB card no. 00-018-1472). Distinctive peaks at $2\theta = 33.78$, 43.96, 48.58, and 57.71 referred to hkl of (112), (122), (023), and (132) for orthorhombic YIG; while distinctive peaks at $2\theta = 20.54$ and 29.21 referred to hkl of (220) and (400) for cubic YIG [43]. Meanwhile, the diffraction peaks at $2\theta = 26.37$ and 43.96 referred to the hkl of (002) and (101) for multi-walled CNT [44]. The phase analysis could also provide the ratio of grown CNT and YIG in the nanohybrid. Based on the Whole Powder Pattern Fitting (WPPF) method, the weight fraction could be calculated from information about the crystal system and lattice constants of the materials. Analysis results using the WPPF method for the nanohybrid were tabulated in Table 1. The weight fraction of CNT was calculated to be 86.0 %, while the remaining 9.6 % and 4.4 % were the weight fractions of orthorhombic and cubic YIG respectively, that served as catalysts.

Fig. 3(a) displayed the micrographs of the YIG nanopowders as the catalyst. The average of the nanoparticles' sizes in the starting powders of YIG was 27 nm, as shown in the particle size distribution from Fig. 3(b). Due to the nature of the particles, which were on the nanometer scale and were known to have magnetic properties, some agglomeration can be observed as well. It can also be concluded from Fig. 3(c) that the morphological structures of CNT synthesized at 900 °C were a mixture of straight, coiled, and twisted tubes with different tube diameters, which was related to the catalyst particles' size and agglomeration [45]. CNT formations depended on the strong catalytic anisotropy of carbon deposition between different crystal faces [39]. The commonly proposed mechanisms for the growth of carbon nanotubes involved the absorption and dissociation of a carbon precursor on the catalyst particle's surface, followed by the dissolution of carbon into the catalyst particle [46]. Although nanotube-like formation can be observed, further characterization using HRTEM was deemed important to investigate the inner structure of the materials and to confirm the CNT growth by observing tube walls and hollowness.

From the HRTEM image in Fig. 4(a), it was observed that the diameter of the smallest nanotube measured was 17.61 nm for CNT-YIG, while the graphitic structure of the grown CNT was displayed in Fig. 4(b). The HRTEM image of CNT-YIG sintered at 900 °C showed the formation of bamboo-like structures of CNT, indicating complete growth of CNT at the said temperature. The sintering temperatures required to form a pure garnet phase for YIG nanoparticles were mentioned as 750 °C for SG (Sol-Gel) and 1000 °C for SS

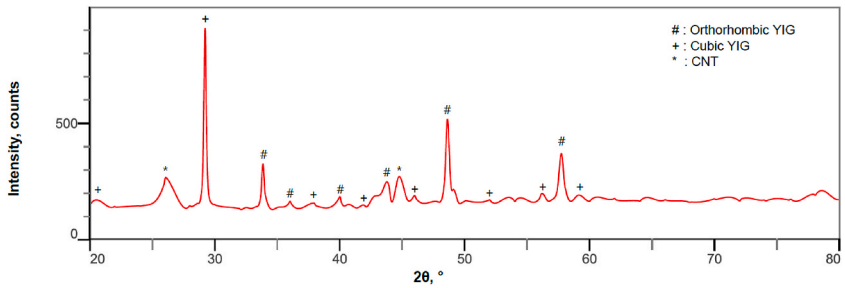

Fig. 2. XRD spectrum of the synthesized CNT-YIG nanohybrid.

Table 1
WPPF analysis results of the CNT-YIG nanohybrid.

Phase/Dataset	CNT	Orthorhombic YIG	Cubic YIG
Weight fraction, wt%	86.0	9.6	4.4
a, Å	2.495	5.011	12.2183
b, Å	2.495	5.653	12.2183
c, Å	6.753	7.498	12.2183
α, °	90.000	90.000	90.000
β, °	90.000	90.000	90.000
γ, °	120.000	90.000	90.000
Lattice volume, $Å^3$	36.397	212.384	1824.044
Strain, %	0.090	0.227	0.235

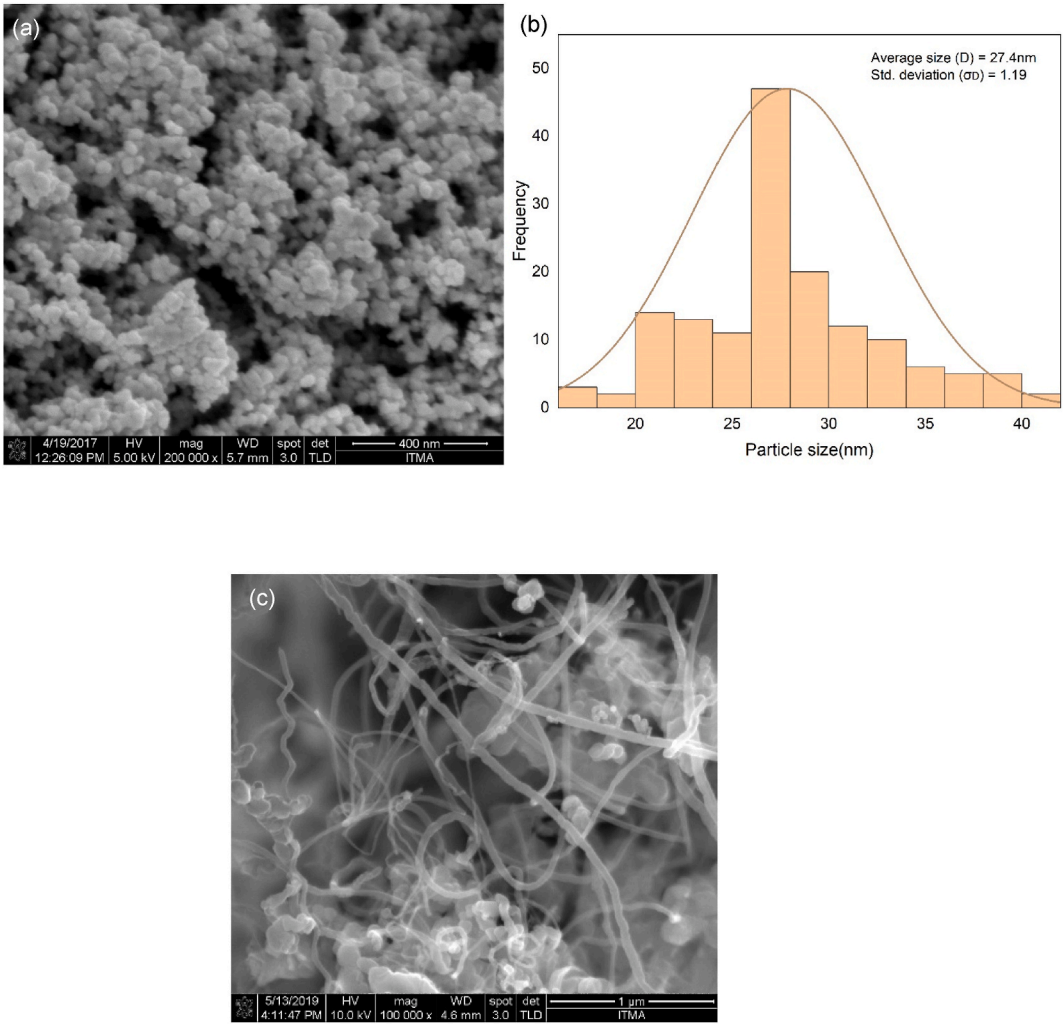

Fig. 3. FESEM micrographs of (a) YIG nanopowders as the starting powders, (b) particle size distribution, and (c) CNT-YIG synthesized at 900 °C.

NPs (Solvent Synthesis Nanoparticles). It was important to note that the sintering temperature was not the same as melting point but was related to the process of forming solid material under heat without melting it to the point of liquefaction [47].

The melting point of nanoparticles can be different from that of micrometer-sized or bulk materials due to the size-dependent properties exhibited at the nanoscale. The phenomenon known as "melting point depression" occurred in nanoparticles, where the melting point of the material decreased as the particle size decreased. This was due to the higher surface area-to-volume ratio in nanoparticles, which altered the thermodynamic stability of the particles, making them melt at lower temperatures compared to their bulk counterparts. Therefore, in this situation, the YIG nanopowders trapped inside the nanotubes were melted, producing the solid, elongated particles in the nanotubes.

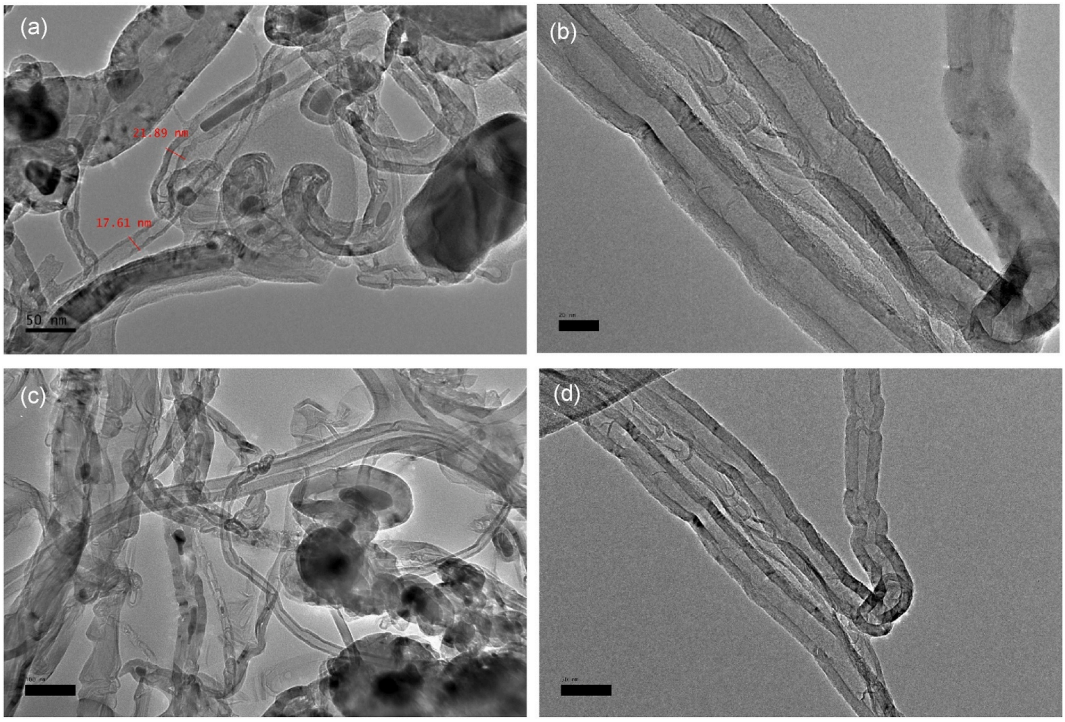

Fig. 4. HRTEM images of CNT-YIG nanohybrid: (a) diameter of CNT, (b) graphitic structure of CNT, (c) bamboo-like structures of CNT at 25,000 magnifications, and (d) bamboo-like structures of CNT at 50,000 magnifications.

Meanwhile, the thermodynamic stability of the CNT also played an important role in their formation. It was understood from Ref. [48] that the shape formation energy was dependent on the formation temperature and catalyst. If the shape formation energy deviated downwards below the threshold conditions, the formation of CNT became unstable and resulted in shape deformation (coil or spiral shape). The synthesis temperature for the previously reported work was 750 °C–800 °C, resulting in coil shaped CNT. As for this work, the temperature was increased to 900 °C; therefore, the formation of straight CNT could be observed as it was closer to 1500K (approximately 1200 °C) [39].

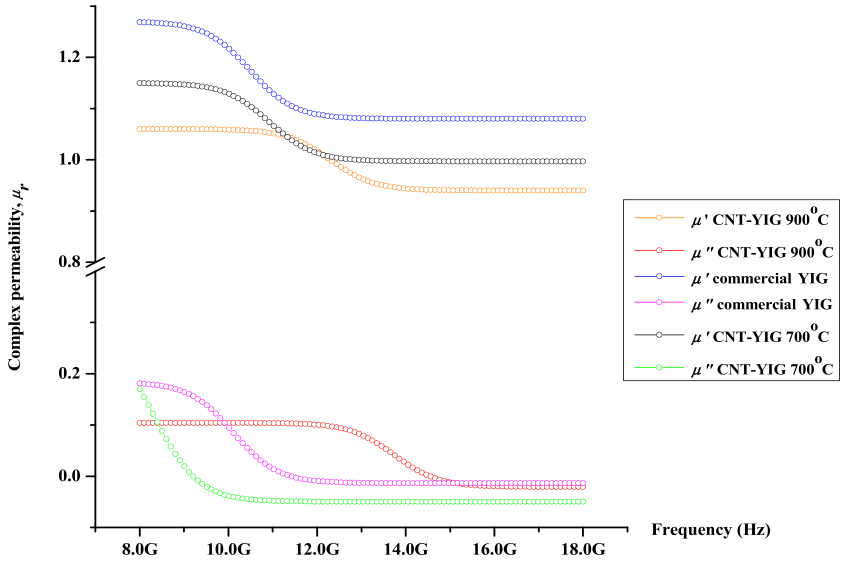

Fig. 5. Complex permeability of (a) commercial YIG, (b) CNT-YIG 700 °C and (c) CNT-YIG 900 °C.

3.3. Complex permeability, complex permittivity, and loss tangent

Generally, the real parts (μ' and ε') exemplify the storage capability of magnetic and electric energy, while the imaginary parts (μ" and ε") indicate the loss of magnetic and electric energy [49]. The permeability spectra of commercial YIG, YIG-CNT 700 °C (for comparison purposes), and YIG-CNT 900 °C in the frequency range from 8 to 18 GHz were exposed in Fig. 5. The relative permeability, μ_r, was written by using Eq. (1):

$$\mu_r = \mu' - j\mu'' \quad \text{(Eq. 1)}$$

The values of μ' and μ'' were about 1.07–1.27 and 0.10 to 0.19, showing a decreasing trend from the low-frequency band to the high-frequency band. The decrease in μ' and μ'' values was explained by the magnetization relaxation due to the displacement of the magnetic domain wall at low frequencies and spin rotation at high frequencies in the sample.

The relative permittivity, ε_r, was defined and given by Eq. (2):

$$\varepsilon_r = \varepsilon' - j\varepsilon'' \quad \text{(Eq. 2)}$$

The complex permittivity spectra of commercial YIG, YIG-CNT 700 °C and YIG-CNT 900 °C were presented in Fig. 6, indicating the positive ε' value in the measured frequency ranged from 8 to 18 GHz. The ε' decreased with increasing frequency, as shown in Fig. 6, and the positive ε' indicated that they were equivalent to micro-capacitors. The interface area increased with increasing carbon content in YIG-CNT 700 °C and YIG-CNT 900 °C, which resulted in the equivalent micro-capacitors, hence increasing the permittivity value [50]. The ε" value for commercial YIG resulted from electron hopping where energy was required, hence giving a certain value. For the YIG-CNT 700 °C and YIG-CNT 900 °C samples, however, the ε" value increased due to the increase in energy through higher electron hopping in the presence of multi-walled carbon nanotube (MWCNT) material. The ε" values of YIG-CNT 700 °C and YIG-CNT 900 °C also specified a decreasing trend versus frequency changes, which was due to the orientation/dipolar polarization mechanism.

Fig. 7 demonstrated the dielectric loss tangent (*tan* δ_ε) and magnetic loss tangent (*tan* δ_μ) of commercial YIG, CNT-YIG 700 °C and CNT-YIG 900 °C, respectively. The value of *tan* δ_ε lied within the range of 0.04–0.25, while *tan* δ_μ had an average value of 0.075–0.12. The loss tangents were obtained by calculating the ratio of imaginary to the real part of permittivity and permeability, as can be defined with Eq. (3):

$$\tan\delta_\varepsilon = \frac{\varepsilon''}{\varepsilon'} \text{ and } \tan\ \delta_\mu = \frac{\mu''}{\mu'} \quad \text{(Eq. 3)}$$

where μ' is real permeability, μ" is imaginary permeability, ε' is real permittivity, and ε" is imaginary permittivity.

The CNT-YIG 900 °C retained a higher *tan* δ_ε compared to *tan* δ_μ at 8–12 GHz, which indicated that the electromagnetic wave absorption was contributed by a dielectric loss mechanism rather than a magnetic loss mechanism.

3.4. Electrical conductivity

IV measurement was conducted using a Keithley 2450 2-point probe to measure the change in electrical current related to the input voltage. Based on the results shown in Fig. 8 and prior characterization of the materials, it can be concluded that the CNT-YIG nanohybrid with high growth temperature (900 °C) showed notable IV characteristics, which confirmed that the material was semi-conductive, although not as conductive as pure CNT. This is due to the composition of the nanohybrid, which consisted of CNT

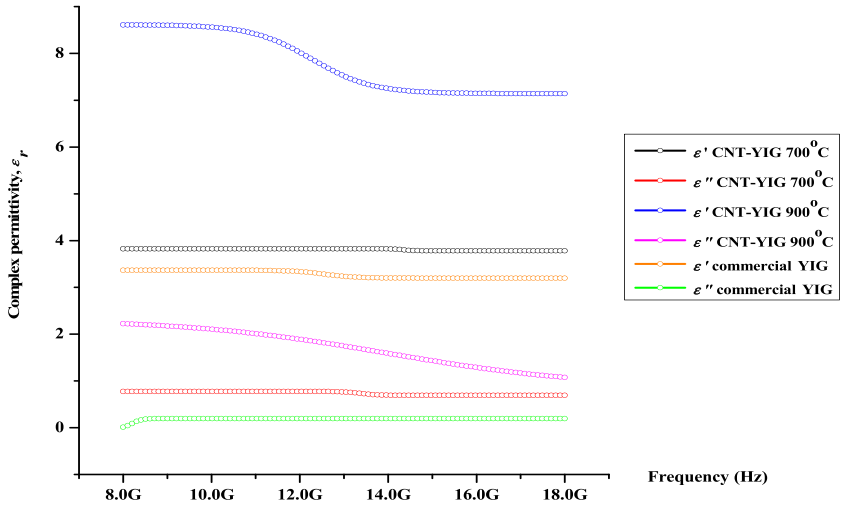

Fig. 6. Complex permittivity of (a) commercial YIG, (b) CNT-YIG 700 °C and (c) CNT-YIG 900 °C.

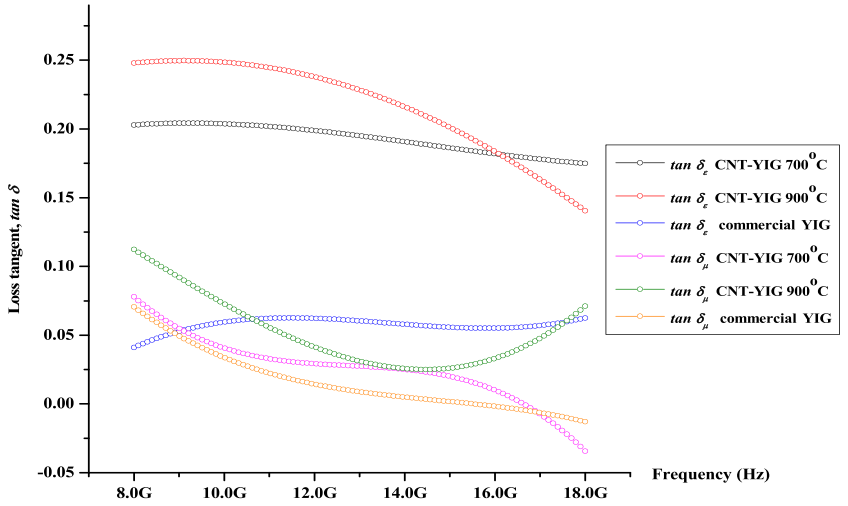

Fig. 7. Dielectric and magnetic loss tangent of (a) commercial YIG, (b) CNT-YIG 700 °C and (c) CNT-YIG 900 °C.

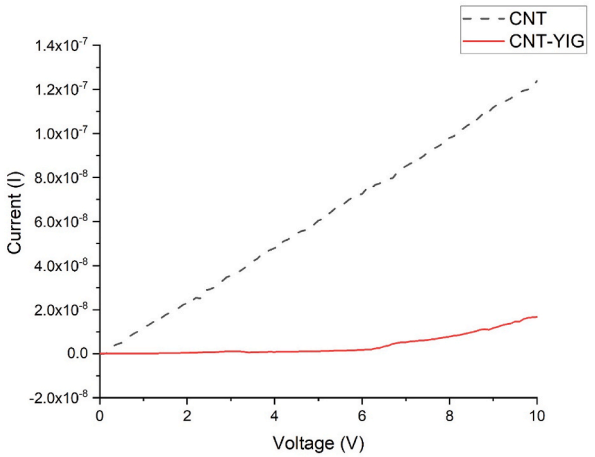

Fig. 8. I-V characteristics of the CNT-YIG nanohybrid.

and the remaining YIG nanopowders, which were still embedded in the materials. Therefore, the material was a non-ohmic conductor, which referred to a material that does not follow Ohm's law of having linear resistance or a consistent relationship between voltage and current. Instead, as can be observed from the graph, the material had high resistance at low voltage, but when it exceeded 6 V, it became a low-resistance material. One example of an application for this type of material is a varistor, which is used for the protection of line transients.

Meanwhile, measurements of other electrical properties such as resistivity, conductivity, and resistance sheet were carried out using a resistivity meter that utilized the 4-point probe method. The CNT-YIG nanohybrid with a growth temperature of 900 °C had a resistance (R) of 2.02×10^3 Ω, a resistance sheet (R_s) of 8.11×10^3 Ω/sq, a resistivity (R_v) of 16.23 Ω cm and a conductivity (S) of 6.17×10^{-2} S/cm. The low conductivity result was expected, as indicated by the IV graph and semiconductive behavior, apart from having YIG nanoparticles in the nanohybrid.

3.5. Potential application as a patch antenna

Based on the characterization and analysis performed on the nanohybrid, it was hypothesized that the materials could be used as the radiating patch of a microstrip patch antenna (MPA) due to their electrical, dielectric, and magnetic properties. Fig. 9 showed the measurement of fabricated MPA using the CNT-YIG nanohybrid with a CNT and YIG antenna as comparison, while Table 2 summarized the measured results of the MPA samples.

Return loss or S_{11} parameter of antenna refers to the power being reflected back from the antenna to the port. It is calculated by using the equation below:

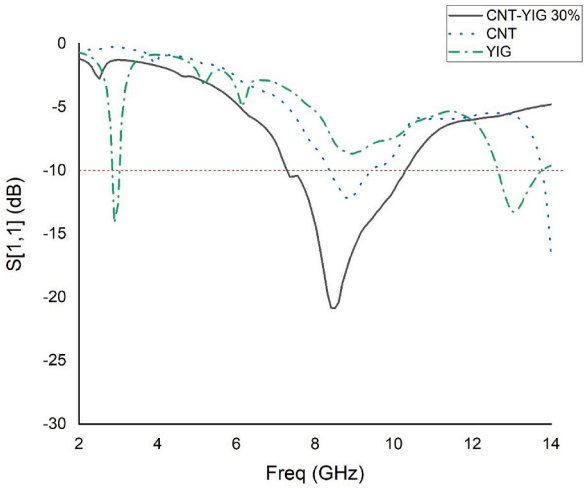

Fig. 9. Return loss measurement of the CNT-YIG patch antenna.

Table 2
Summary of CNT-YIG nanohybrid MPA measurement results.

MPA Sample	Center frequency, f_c (GHz)	Return loss (RL), S_{11} (dB)	−10dB Bandwidth (GHz)	Fractional Bandwidth, FBW (%)
CNT	8.790	−12.16	1.14	12.96
YIG	8.885	−8.66	n/a	n/a
CNT-YIG	8.505	−20.86	3.01	34.22

$$RL\ (dB) = 10\ log_{10}\frac{P_i}{P_r} \tag{4}$$

Where P_i is the incident power and P_r is the reflected power.

Meanwhile, the −10 dB bandwidth is calculated from the upper frequency (f_1) and lower frequency (f_2), where the return loss is −10 dB.

Then, the fractional bandwidth (FBW) can be calculated using the equation below:

$$FBW\ (\%) = \frac{f_1 - f_2}{f_c} \times 100 \tag{5}$$

Since CNT-YIG had lower conductivity than CNT, the center frequency (f_c) of CNT-YIG MPA was slightly shifted to a lower frequency, of which the measured result is 8.505 GHz. This result indicated that the antenna design can be further miniaturized to shift to higher frequencies, especially for those researchers who aim to work in the terahertz region but cannot execute them due to the restriction of the materials used.

The CNT-YIG hybrid, functioning as the radiating patch, demonstrated that the material's combination of electric, dielectric, and magnetic characteristics was what caused the larger fringing fields. Compared to the MPA utilizing CNT as the radiating patch, the combined qualities enabled the antenna to look bigger in terms of electric fields, hence widening the bandwidth.

The result obtained supported this theory, of which the −10 dB bandwidth of CNT-YIG MPA is wider than the CNT MPA, resulting in a higher fractional bandwidth (FBW) of 34.22 % for CNT-YIG MPA. The result also agreed with other literature reported data involving the use of CNT-ferrite nanohybrid [46,51–53] with reported bandwidth ranging from 1 GHz up to 3 GHz.

In terms of the return loss, the CNT-YIG MPA sample exhibited superior return loss in comparison to the CNT MPA, which was the control sample. MPA using CNT-YIG synthesized at 900 °C displayed a better return loss or reflection coefficient, which was contributed by the conductivity of the sample, and the amount of CNT growth hybridized with YIG as a catalyst. It has been concluded that CNT-YIG samples with high sintering temperatures promoted better or longer CNT growth. This result could lead to better continuity of power transmission and higher reflected power. The results also indicated that the improved return loss and wider bandwidth were influenced by the impedance matching attributed to magnetic and dielectric coupling derived from the nanohybrid and the high values of dielectric and magnetic loss tangents of the CNT-YIG nanohybrid.

4. Conclusion

This paper demonstrated the success of CNT-YIG nanohybrid powder synthesis using the CVD method. The results indicated that the growth of CNT from YIG nanopowders as catalysts with a synthesis temperature of 900 °C exhibited graphitization, leading to

increased conductivity of the nanohybrid material as compared to the starting ferrite catalyst. The nanohybrid also exhibited improved electromagnetic properties, with the nanohybrid having higher permittivity, dielectric, and magnetic loss tangents. The CNT-YIG nanohybrid thick film paste produced was then used as the radiating patch of the MPA by utilizing the screen-printing technique. According to the results of the antenna measurement, the CNT-YIG nanohybrid's combined electrical, dielectric, and magnetic properties greatly increased the antenna's bandwidth to 3.01 GHz, demonstrating a greater bandwidth than the control sample, which only has a 1.14 GHz bandwidth. The results showed that the enhanced conductivity of the CNT grown from the ferrite catalyst, as well as its improved dielectric and magnetic properties, demonstrated that the CNT-ferrite nanohybrid can be further investigated as an element in patch antenna fabrication or any other application involving electromagnetic parameters because of its exceptional and distinctive properties.

CRediT authorship contribution statement

Intan Helina Hasan: Writing – original draft, Resources, Project administration, Methodology, Investigation, Funding acquisition, Formal analysis, Data curation, Conceptualization. **Ismayadi Ismail:** Writing – review & editing, Validation, Formal analysis, Conceptualization. **Mohd Nizar Hamidon:** Writing – review & editing, Supervision, Project administration, Methodology, Formal analysis. **Muhammad Syazwan Mustaffa:** Validation, Formal analysis, Data curation. **Nor Hapishah Abdullah:** Investigation, Formal analysis, Data curation. **Farah Nabilah Shafiee:** Methodology, Investigation, Formal analysis, Data curation.

Declaration of competing interest

The authors declare that they have no known competing financial interests or personal relationships that could have appeared to influence the work reported in this paper.

Acknowledgment

The authors wish to thank the students and staff of the Institute of Nanoscience and Nanotechnology (ION2), UPM for their help and support during the project. This project is funded by Universiti Putra Malaysia, under the Geran Putra fund (GP-9627100).

References

[1] G.W. Hanson, Fundamental transmitting properties of carbon nanotube antennas, IEEE Trans Antennas Propag 53 (2005) 3426–3435, https://doi.org/10.1109/TAP.2005.858865.
[2] G.W. Hanson, Current on an infinitely-long carbon nanotube antenna excited by a gap generator, IEEE Trans Antennas Propag 54 (2006) 76–81, https://doi.org/10.1109/TAP.2005.861550.
[3] T.A. Elwi, H.M. Al-Rizzo, D.G. Rucker, E. Dervishi, Z. Li, A.S. Biris, Multi-walled carbon nanotube-based RF antennas, Nanotechnology 21 (2010) 045301, https://doi.org/10.1088/0957-4484/21/4/045301.
[4] K.S. Chaya Devi, B. Angadi, H.M. Mahesh, Multiwalled carbon nanotube-based patch antenna for bandwidth enhancement, Mater. Sci. Eng., B 224 (2017) 56–60, https://doi.org/10.1016/j.mseb.2017.07.005.
[5] B. Aïssa, M. Nedil, M.a. Habib, E. Haddad, W. Jamroz, D. Therriault, Y. Coulibaly, F. Rosei, Fluidic patch antenna based on liquid metal alloy/single-wall carbon-nanotubes operating at the S-band frequency, Appl. Phys. Lett. 103 (2013), https://doi.org/10.1063/1.4817861.
[6] S.D. Keller, A.I. Zaghloul, Multifunctional meshed carbon nanotube thread patch antenna, in: 2011 IEEE SENSORS Proceedings, IEEE, 2011, pp. 631–634, https://doi.org/10.1109/ICSENS.2011.6127180.
[7] S.D. Keller, A.I. Zaghloul, V. Shanov, M.J. Schulz, D.B. Mast, N.T. Alvarez, Radiation performance of polarization selective carbon nanotube sheet patch antennas, IEEE Trans Antennas Propag 62 (2014) 48–55, https://doi.org/10.1109/TAP.2013.2287272.
[8] Y. Jia, Y. Chen, H. Jiang, Y. Le, H. Lin, A carbon nanotube patch antenna for polarization selective radiation performance, in: 2018 1st IEEE International Conference on Knowledge Innovation and Invention (ICKII), IEEE, 2018, pp. 217–220, https://doi.org/10.1109/ICKII.2018.8569112.
[9] P. Savi, K. Naishadam, A. Bayat, M. Giorcelli, S. Quaranta, Multi-Walled Carbon Nanotube thin film loading for tuning microstrip patch antennas, in: 2016 10th European Conference on Antennas and Propagation, EuCAP, 2016, 2016, https://doi.org/10.1109/EuCAP.2016.7481993.
[10] K. Naishadham, An investigation on the tuning of a microstrip patch antenna using carbon nanotube thin films, in: 2014 IEEE Antennas and Propagation Society International Symposium (APSURSI), IEEE, 2014, pp. 900–901, https://doi.org/10.1109/APS.2014.6904778.
[11] M.M. Mansor, S.K.A. Rahim, U. Hashim, A CPW-fed 2.45 GHz wearable Antenna using conductive nanomaterials for on-body applications, in: IEEE TENSYMP 2014 - 2014 IEEE Region 10 Symposium, 2014, pp. 240–243, https://doi.org/10.1109/tenconspring.2014.6863034.
[12] H.L. Yang, Y. Chen, C.Q. Li, G. Wu, J.N. Wang, Cellular-structured carbon nanotube composite films with broadband microwave absorption and shape memory, Carbon N Y 210 (2023) 118079, https://doi.org/10.1016/J.CARBON.2023.118079.
[13] A. Saini, A. Thakur, P. Thakur, Effective permeability and miniaturization estimation of ferrite-loaded microstrip patch antenna, J. Electron. Mater. 45 (2016) 4162–4170, https://doi.org/10.1007/s11664-016-4634-y.
[14] M.A. Amiri, C.A. Balanis, C.R. Birtcher, Gain and bandwidth enhancement of ferrite-loaded CBS antenna using material shaping and positioning, IEEE Antennas Wirel Propag Lett 12 (2013) 611–614, https://doi.org/10.1109/LAWP.2013.2260519.
[15] K. Borah, N. Bhattacharyya, Magneto-dielectric material with nano ferrite inclusion for microstrip antennas: dielectric characterization, IEEE Trans. Dielectr. Electr. Insul. 17 (2010), https://doi.org/10.1109/TDEI.2010.5658216.
[16] F.Z. Hanin, Performance of Patch Antenna Loaded of Ferrites Films, 2014, pp. 2–4.
[17] S.S. Pattnaik, R.K. Mishra, N. Das, Elliptical microstrip antenna on ferrite substrate, Electron. Lett. 26 (1990).
[18] S.N. Das, S.K. Chowdhury, Rectangular microstrip antenna on a ferrite substrate, IEEE Trans Antennas Propag 30 (1982) 499–502, https://doi.org/10.1109/TAP.1982.1142816.
[19] A. Rahman, N.M. Yi, A.U. Ahmed, T. Alam, M.J. Singh, M.T. Islam, A compact 5G antenna printed on manganese zinc ferrite substrate material, IEICE Electron. Express 13 (2016), https://doi.org/10.1587/elex.13.20160377.
[20] S. Bae, Y.K. Hong, A. Lyle, Effect of Ni–Zn ferrite on bandwidth and radiation efficiency of embedded antenna for mobile phone, J. Appl. Phys. 103 (2008) 07E929, https://doi.org/10.1063/1.2838619.
[21] P. Parsons, K. Duncan, A. Giri, J.Q. Xiao, S.P. Karna, NiZn ferrite nanoparticles and their polymer composites for antenna miniaturization, in: Proceedings of the IEEE Conference on Nanotechnology, 2012, https://doi.org/10.1109/NANO.2012.6322191.

[22] I.H. Hasan, M.N. Hamidon, A. Ismail, I. Ismail, N.A. Mohd Azhari, M.A. Mohd Kusaimi, S. Azhari, Nickel zinc ferrite thick film with linseed oil as organic vehicle for microwave device applications, Mater. Chem. Phys. 236 (2019), https://doi.org/10.1016/j.matchemphys.2019.121790.

[23] I.H. Hasan, M.N. Hamidon, A. Ismail, I. Ismail, A.S. Mekki, M.A. Mohd Kusaimi, S. Azhari, R. Osman, YIG thick film as substrate overlay for bandwidth enhancement of microstrip patch antenna, IEEE Access 6 (2018) 32601–32611, https://doi.org/10.1109/ACCESS.2018.2842749.

[24] S. Kumar, R. Walia, A. Kumar, V. Verma, Hybrid structure of MWCNT/ferrite and GO incorporated composites for microwave shielding properties and their practical applications, RSC Adv. 11 (2021) 9775–9787, https://doi.org/10.1039/D1RA01129D.

[25] J. Zhang, R. Shu, C. Guo, R. Sun, Y. Chen, J. Yuan, Fabrication of nickel ferrite microspheres decorated multi-walled carbon nanotubes hybrid composites with enhanced electromagnetic wave absorption properties, J. Alloys Compd. 784 (2019) 422–430, https://doi.org/10.1016/j.jallcom.2019.01.073.

[26] M.Z. Ashfaq, A. Ashfaq, M.K. Majeed, A. Saleem, S. Wang, M. Ahmad, M.M. Hussain, Y. Zhang, H. Gong, Confined tailoring of CoFe2O4/MWCNTs hybrid-architectures to tune electromagnetic parameters and microwave absorption with broadened bandwidth, Ceram. Int. 48 (2022) 9569–9578, https://doi.org/10.1016/j.ceramint.2021.12.155.

[27] H. Hosseini, H. Mahdavi, Nanocomposite based on epoxy and MWCNTs modified with NiFe2O4 nanoparticles as efficient microwave absorbing material, Appl. Organomet. Chem. 32 (2018) e4294, https://doi.org/10.1002/aoc.4294.

[28] L. Yu, S. Ahmad, S. Appadu, I. Kong, M. Tarawneh, M. Flaifel, Comparison of magnetic and microwave absorbing properties between multiwalled carbon nanotubes nanocomposite, nickel zinc ferrite nanocomposite and hybrid nanocomposite, World Journal of Engineering 11 (2014) 317–322, https://doi.org/10.1260/1708-5284.11.4.317.

[29] S.S. Raut, B.R. Sankapal, M.S.A. Hossain, S. Pradhan, R.R. Salunkhe, Y. Yamauchi, Zinc ferrite anchored multiwalled carbon nanotubes for high-performance supercapacitor applications, Eur. J. Inorg. Chem. 2018 (2018) 137–142, https://doi.org/10.1002/ejic.201700836.

[30] S.H. Siddiki, S. Das, K. Verma, L. Dashairya, S. Das, V.K. Thakur, G.C. Nayak, Substituted nickel ferrite coated MWCNT/PVDF based epoxy nanocomposite for microwave absorption, Ceram. Int. 48 (2022) 30260–30271, https://doi.org/10.1016/J.CERAMINT.2022.06.299.

[31] J. Sengupta, C. Jacob, The effect of Fe and Ni catalysts on the growth of multiwalled carbon nanotubes using chemical vapor deposition, J. Nanoparticle Res. 12 (2010) 457–465, https://doi.org/10.1007/s11051-009-9667-1.

[32] G. Gorrasi, C. Milone, E. Piperopoulos, R. Pantani, Preparation, processing and analysis of physical properties of calcium ferrite-CNTs/PET nano-composite, Compos. B Eng. 81 (2015) 44–52, https://doi.org/10.1016/j.compositesb.2015.06.019.

[33] L.J. Yu, S.H. Ahmad, I. Kong, S. Appadu, M.H. Flaifel, Magnetic properties, microstructure and morphology of thermoplastic natural rubber composite reinforced with NiZn ferrite/Mwnt, Sains Malays. 41 (2012).

[34] X. Sun, X. Zhu, X. Yang, J. Sun, Y. Xia, D. Yang, CoFe2O4/carbon nanotube aerogels as high performance anodes for lithium ion batteries, Green Energy Environ. 2 (2017) 160–167, https://doi.org/10.1016/j.gee.2017.01.008.

[35] C. Pereira, R.S. Costa, L. Lopes, B. Bachiller-Baeza, I. Rodríguez-Ramos, A. Guerrero-Ruiz, P.B. Tavares, C. Freire, A.M. Pereira, Multifunctional mixed valence N-doped CNT@MFe_2O_4 hybrid nanomaterials: from engineered one-pot coprecipitation to application in energy storage paper supercapacitors, Nanoscale 10 (2018) 12820–12840, https://doi.org/10.1039/c8nr03533d.

[36] R. Mazurenko, S. Prokopenko, M. Godzierz, A. Hercog, A. Kobyliukh, G. Gunja, S. Makhno, U. Szeluga, P. Gorbyk, B. Trzebicka, Polymer nanocomposites based on nanosized substituted ferrites (NiZn)1−xMnxFe2O4 on the surface of carbon nanotubes for effective interaction with high-frequency EM radiation, Materials 17 (2024) 986, https://doi.org/10.3390/ma17050986.

[37] R. Mazurenko, S. Prokopenko, M. Godzierz, A. Hercog, S. Makhno, U. Szeluga, P. Gorbyk, B. Trzebicka, M. Kartel, Synthesis of nanosized spinel ferrites MnFe2O4 on the surface of carbon nanotubes for the creation of polymer composites with enhanced microwave absorption capacity, Appl. Mater. Today 35 (2023) 101972, https://doi.org/10.1016/J.APMT.2023.101972.

[38] R. Mohan, R. Paulose, Influence of ferrites nanoparticles anchored on CNT hybrid nanocomposites for high-performance energy storage applications, J. Electron. Mater. 47 (2018) 6878–6885, https://doi.org/10.1007/s11664-018-6615-9.

[39] L. Liu, J. Zhao, Toroidal and coiled carbon nanotubes, in: S. Suzuki (Ed.), Syntheses and Applications of Carbon Nanotubes and Their Composites, IntechOpen, Rijeka, 2013, https://doi.org/10.5772/51125. Ch. 12.

[40] I.H. Hasan, M.N. Hamidon, A. Ismail, I. Ismail, N.A. Mohd Azhari, M.A. Mohd Kusaimi, S. Azhari, Nickel zinc ferrite thick film with linseed oil as organic vehicle for microwave device applications, Mater. Chem. Phys. 236 (2019), https://doi.org/10.1016/j.matchemphys.2019.121790.

[41] I.H. Hasan, M.N. Hamidon, A. Ismail, I. Ismail, M.A.M. Kusaimi, S. Azhari, N.A.M. Azhari, R. Osman, Nickel zinc ferrite thick film as substrate overlay for improved performance of microstrip patch antenna, in: IOP Conf Ser Mater Sci Eng, 2018, https://doi.org/10.1088/1757-899X/380/1/012004.

[42] O.A. Maslova, A.S. Mikheikin, I.N. Leontiev, Y.I. Yuzyuk, A.G. Tkachev, Raman spectra of Taunit carbon nanomaterial, Nanotechnol Russ 5 (2010), https://doi.org/10.1134/S1995078010090089.

[43] M.A. Musa, R.S. Azis, N.H. Osman, J. Hassan, T. Zangina, Structural and magnetic properties of yttrium iron garnet (YIG) and yttrium aluminum iron garnet (YAlG) nanoferrite via sol-gel synthesis, Results, Phys 7 (2017) 1135–1142, https://doi.org/10.1016/j.rinp.2017.02.038.

[44] F.H. Abdulrazzak, A.F. Alkiam, F.H. Hussein, Behavior of X-ray analysis of carbon nanotubes, in: H.E.-D. Saleh, S.M.M. El-Sheikh (Eds.), Perspective of Carbon Nanotubes, IntechOpen, Rijeka, 2019, https://doi.org/10.5772/intechopen.85156. Ch. 7.

[45] N.A. Algadri, Z. Hassan, K. Ibrahim, M. Bououdina, Effect of ferrocene catalyst particle size on structural and morphological characteristics of carbon nanotubes grown by microwave oven, J. Mater. Sci. 52 (2017) 12772–12782, https://doi.org/10.1007/s10853-017-1381-2.

[46] N. Rosdi, R.S. Azis, I. Ismail, N. Mokhtar, M.M. Muhammad Zulkimi, M.S. Mustaffa, Structural, microstructural, magnetic and electromagnetic absorption properties of spiraled multiwalled carbon nanotubes/barium hexaferrite (MWCNTs/BaFe12O19) hybrid, Sci. Rep. 11 (2021) 15982, https://doi.org/10.1038/s41598-021-95332-9.

[47] V. Sharma, J. Saha, S. Patnaik, B.K. Kuanr, Synthesis and characterization of yttrium iron garnet (YIG) nanoparticles - microwave material, AIP Adv. 7 (2016) 056405, https://doi.org/10.1063/1.4973199.

[48] O.-Y. Zhong-can, Z.-B. Su, C.-L. Wang, Coil Formation in multishell carbon nanotubes: competition between curvature elasticity and interlayer adhesion, Phys. Rev. Lett. 78 (1997) 4055–4058, https://doi.org/10.1103/PhysRevLett.78.4055.

[49] S. Tyagi, H.B. Baskey, R.C. Agarwala, V. Agarwala, T.C. Shami, Development of hard/soft ferrite nanocomposite for enhanced microwave absorption, Ceram. Int. 37 (2011) 2631–2641, https://doi.org/10.1016/j.ceramint.2011.04.012.

[50] H. Gu, J. Guo, Q. He, Y. Jiang, Y. Huang, N. Haldolaarachige, Z. Luo, D.P. Young, S. Wei, Z. Guo, Magnetoresistive polyaniline/multi-walled carbon nanotube nanocomposites with negative permittivity, Nanoscale 6 (2014) 181–189, https://doi.org/10.1039/C3NR04152B.

[51] M.M. Syazwan, A.N. Hapishah, M.N. Hamidon, I. Ismail, I.H. Hasan, Design and development of Ni0.75Zn0.25Fe2O4/MWCNT microstrip patch antenna (MPA) for ISM band spectrum applications, Synth. Met. 271 (2021) 116630, https://doi.org/10.1016/j.synthmet.2020.116630.

[52] M.S. Mustaffa, R.S. Azis, N.H. Abdullah, I. Ismail, I.R. Ibrahim, An investigation of microstructural, magnetic and microwave absorption properties of multi-walled carbon nanotubes/Ni0.5Zn0.5Fe2O4, Sci. Rep. 9 (2019) 15523, https://doi.org/10.1038/s41598-019-52233-2.

[53] M.M.M. Zulkimi, R.S. Azis, I. Ismail, N. Mokhtar, M. Ertugrul, M.N. Hamidon, I.H. Hasan, Y.O. Yesilbag, F.N. Tuzluca, G. Ozturk, U.C. Hasar, Enhancing radar absorption performance of Sr-hexaferrite by hybridization with coiled carbon nanotubes via chemical vapour deposition method, Diam. Relat. Mater. 137 (2023) 110118, https://doi.org/10.1016/j.diamond.2023.110118.